High-order multilayer coated blazed gratings for high resolution soft x-ray spectroscopy

Dmitriy L. Voronov,[1,*] Leonid I. Goray,[2,3] Tony Warwick,[1] Valeriy V. Yashchuk[1], and Howard A. Padmore[1]

[1]*Lawrence Berkeley National Laboratory, Berkeley, California, 94720, USA*
[2]*Saint Petersburg Academic University, Khlopina 8/3, St. Petersburg, 194021, Russia*
[3]*Institute for Analytical Instrumentation, Rizhsky Prospect 26, St. Petersburg, 190103, Russia*
**dlvoronov@lbl.gov*

Abstract. A grand challenge in soft x-ray spectroscopy is to drive the resolving power of monochromators and spectrometers from the 10^4 achieved routinely today to well above 10^5. This need is driven mainly by the requirements of a new technique that is set to have enormous impact in condensed matter physics, Resonant Inelastic X-ray Scattering (RIXS). Unlike x-ray absorption spectroscopy, RIXS is not limited by an energy resolution dictated by the core-hole lifetime in the excitation process. Using much higher resolving power than used for normal x-ray absorption spectroscopy enables access to the energy scale of soft excitations in matter. These excitations such as magnons and phonons drive the collective phenomena seen in correlated electronic materials such as high temperature superconductors. RIXS opens a new path to study these excitations at a level of detail not formerly possible. However, as the process involves resonant excitation at an energy of around 1 keV, and the energy scale of the excitations one would like to see are at the meV level, to fully utilize the technique requires the development of monochromators and spectrometers with one to two orders of magnitude higher energy resolution than has been conventionally possible. Here we investigate the detailed diffraction characteristics of multilayer blazed gratings. These elements offer potentially revolutionary performance as the dispersive element in ultra-high resolution x-ray spectroscopy. In doing so, we have established a roadmap for the complete optimization of the grating design. Traditionally 1st order gratings are used in the soft x-ray region, but we show that as in the optical domain, one can work in very high spectral orders and thus dramatically improve resolution without significant loss in efficiency.

OCIS codes: (050.1950) Diffraction gratings; (340.7480) X-rays, soft x-rays, extreme ultraviolet (EUV).

References and links

1. V. V. Martynov, H. A. Padmore, A. Yuakshin, and Y. A. Agafonov, "Lamellar multilayer gratings with very high diffraction efficiency," Proc. SPIE **3150**, 2–8 (1997).
2. D. L. Voronov, R. Cambie, R. M. Feshchenko, E. Gullikson, H. A. Padmore, A. V. Vinogradov, and V. V. Yashchuk, "Development of an ultra-high resolution diffraction grating for soft X-rays," Proc. SPIE **6705**, 67050E, 67050E-12 (2007).
3. I. V. Kozhevnikov, R. van der Meer, H. M. J. Bastiaens, K.-J. Boller, and F. Bijkerk, "Analytic theory of soft x-ray diffraction by Lamellar Multilayer Gratings," Opt. Express **19**(10), 9172–9184 (2011).
4. R. van der Meer, B. Krishnan, I. V. Kozhevnikov, M. J. De Boer, B. Vratzov, H. M. J. Bastiaens, J. Huskens, W. G. van der Wiel, P. E. Hegeman, G. C. S. Brons, K.-J. Boller, and F. Bijkerk, "Improved resolution for soft-x-ray monochromatization using lamellar multilayer gratings," Proc. SPIE **8139**, 81390Q (2011).
5. M. Ahn, R. K. Heilmann, and M. L. Schattenburg, "Fabrication of 200 nm-period blazed transmission gratings on silicon-on-insulator wafers," J. Vac. Sci. Technol. B **26**(6), 2179–2182 (2008).

#221162 - $15.00 USD Received 20 Aug 2014; revised 7 Jan 2015; accepted 20 Jan 2015; published 17 Feb 2015

6. R. K. Heilmann, M. Ahn, A. Bruccoleri, C.-H. Chang, E. M. Gullikson, P. Mukherjee, and M. L. Schattenburg, "Diffraction efficiency of 200-nm-period critical-angle transmission gratings in the soft x-ray and extreme ultraviolet wavelength bands," Appl. Opt. **50**(10), 1364–1373 (2011).
7. Y. V. Shvyd'ko, M. Lerche, U. Kuetgens, H. D. Rüter, A. Alatas, and J. Zhao, "X-ray Bragg diffraction in asymmetric backscattering geometry," Phys. Rev. Lett. **97**(23), 235502 (2006).
8. J. C. Rife, W. R. Hunter, T. W. Barbee, Jr., and R. G. Cruddace, "Multilayer-coated blazed grating performance in the soft x-ray region," Appl. Opt. **28**(15), 2984–2986 (1989).
9. M. Nevière, "Multilayer coated gratings for x-ray diffraction: differential theory," J. Opt. Soc. Am. A **8**(9), 1468–1473 (1991).
10. J. H. Underwood, C. Kh. Malek, E. M. Gullikson, and M. Krumrey, "Multilayer-coated echelle gratings for soft x-rays and extreme ultraviolet," Rev. Sci. Instrum. **66**(2), 2147–2150 (1995).
11. M. P. Kowalski, R. G. Cruddace, K. F. Heidemann, R. Lenke, H. Kierey, T. W. Barbee, Jr., and W. R. Hunter, "Record high extreme-ultraviolet efficiency at near-normal incidence from a multilayer-coated polymer-overcoated blazed ion-etched holographic grating," Opt. Lett. **29**(24), 2914–2916 (2004).
12. H. Lin, L. Zhang, L. Li, Ch. Jin, H. Zhou, and T. Huo, "High-efficiency multilayer-coated ion-beam-etched blazed grating in the extreme-ultraviolet wavelength region," Opt. Lett. **33**(5), 485–487 (2008).
13. D. L. Voronov, E. H. Anderson, R. Cambie, S. Cabrini, S. D. Dhuey, L. I. Goray, E. M. Gullikson, F. Salmassi, T. Warwick, V. V. Yashchuk, and H. A. Padmore, "A 10,000 groove/mm multilayer coated grating for EUV spectroscopy," Opt. Express **19**(7), 6320–6325 (2011).
14. D. L. Voronov, E. H. Anderson, E. M. Gullikson, F. Salmassi, T. Warwick, V. V. Yashchuk, and H. A. Padmore, "Ultra-high efficiency multilayer blazed gratings through deposition kinetic control," Opt. Lett. **37**(10), 1628–1630 (2012).
15. Y. Fujii, K. I. Aoyama, and J. I. Minowa, "Optical demultiplexer using a silicon echelette grating," IEEE J. Quantum Electron. **16**(2), 165–169 (1980).
16. P. Philippe, S. Valette, O. M. Mendez, and D. Maystre, "Wavelength demultiplexer: using echelette gratings on silicon substrate," Appl. Opt. **24**(7), 1006–1011 (1985).
17. D. L. Voronov, M. Ahn, E. H. Anderson, R. Cambie, C. H. Chang, E. M. Gullikson, R. K. Heilmann, F. Salmassi, M. L. Schattenburg, T. Warwick, V. V. Yashchuk, L. Zipp, and H. A. Padmore, "High-efficiency 5000 lines/mm multilayer-coated blazed grating for extreme ultraviolet wavelengths," Opt. Lett. **35**(15), 2615–2617 (2010).
18. T. Warwick, H. A. Padmore, D. L. Voronov, V. V. Yashchuk, R. Garrett, I. Gentle, K. Nugent, and S. Wilkins, "A soft x-ray spectrometer using a highly dispersive multilayer grating," AIP Conf. Proc. **1234**, 776–780 (2010).
19. D. L. Voronov, E. M. Gullikson, F. Salmassi, T. Warwick, and H. A. Padmore, "Enhancement of diffraction efficiency via higher-order operation of a multilayer blazed grating," Opt. Lett. **39**(11), 3157–3160 (2014).
20. *http://henke.lbl.gov/*
21. A. P. Lukirskii and E. P. Savinov, "Use of diffraction gratings and echelettes in the ultrasoft x-ray region," Opt. Spectrosc. **14**, 147–151 (1963).
    A. P. Lukirskii, E. P. Savinov, and Yu. P. Shepelev, "Behaviour of gold and titanium coated echelettes in the 23.6-113 A° region," Opt. Spectrosc. **15**, 290–293 (1963).
22. D. Maystre and R. Petit, "Some recent theoretical results for gratings: application for their use in the very far ultraviolet region," Nouv. Rev. Opt. **7**(3), 165–180 (1976).
23. M. Nevière and F. Montiel, "Soft x-ray multilayer coated echelle gratings: electromagnetic and phenomenological study," J. Opt. Soc. Am. A **13**(4), 811–818 (1996).
24. L. I. Goray, "Numerical analysis of the efficiency of multilayer-coated gratings using integral method," Nucl. Instrum. Meth. A **536**(1-2), 211–221 (2005).
25. L. I. Goray, "Scalar and electromagnetic properties of X-ray diffraction gratings," Bull. Russ. Acad. Sci., Physics **69**, 231–236 (2005).
26. *http://www.pcgrate.com/*.
27. L. I. Goray, "Application of the boundary integral equation method to very small wavelength-to-period diffraction problems," Waves Random Media **20**(4), 569–586 (2010).
28. L. I. Goray, "Application of the rigorous method to x-ray and neutron beam scattering," J. Appl. Phys. **108**(3), 033516 (2010).
29. L. I. Goray and G. Schmidt, "Boundary integral equation methods for conical diffraction and short waves," in *Gratings: Theory and Numerical Applications*, E. Popov, ed. (Institute Fresnel, AMU, 2014), pp. 12.1–12.86, *http://www.fresnel.fr/numerical-grating-book-2*.
30. L. I. Goray and G. Schmidt, "Solving conical diffraction grating problems with integral equations," J. Opt. Soc. Am. A **27**(3), 585–597 (2010).
31. A. Rathsfeld, G. Schmidt, and B. H. Kleemann, "On a fast integral equation method for diffraction gratings," Commun. Comput. Phys. **1**, 984–1009 (2006).
32. J. Elschner, R. Hinder, A. Rathsfeld, and G. Schmidt, DIPOG Homepage, *http://www.wias-berlin.de/software/DIPOG*.
33. A. V. Vinogradov and B. Ya. Zeldovich, "X-ray and far UV multilayer mirrors: Principles and possibilities," Appl. Opt. **16**(1), 89–93 (1977).
34. A. V. Vinogradov, I. A. Brytov, A. Ya. Grudsky, M. T. Kogan, I. V. Kozhevnikov, and V. A. Slemzin, *Mirror X-Ray Optics (in Russian)* (Mashinostroenie, 1989).

#221162 - $15.00 USD Received 20 Aug 2014; revised 7 Jan 2015; accepted 20 Jan 2015; published 17 Feb 2015

35. See, for example, Yu. Shvyd'ko, *X-Ray Optics. High-Resolution Applications* (Springer, 2004).
36. L. Goray and M. Lubov, "Nonlinear continuum growth model of multiscale reliefs as applied to rigorous analysis of multilayer short-wave scattering intensity. I. Gratings," J. Appl. Cryst. **46**(4), 926–932 (2013).
37. D. Attwood, *Soft X-Rays and Extreme Ultraviolet Radiation* (Cambridge University, 1999).
38. T. Warwick, Y.-D. Chuang, D. L. Voronov, and H. A. Padmore, "A multiplexed high-resolution imaging spectrometer for resonant inelastic soft X-ray scattering spectroscopy," J. Synchrotron Radiat. **21**(4), 736–743 (2014).
39. V. E. Levashov, E. N. Zubarev, A. I. Fedorenko, V. V. Kondratenko, O. V. Poltseva, S. A. Yulin, I. I. Struk, and A. V. Vinogradov, "High throughput and resolution compact spectrograph for the 124-250 A range based on $MoSi_2$-Si sliced multilayer grating," Opt. Commun. **109**(1-2), 1–4 (1994).
40. R. M. Fechtchenko, A. V. Vinogradov, and D. L. Voronov, "Optical properties of sliced multilayer gratings," Opt. Commun. **210**(3-6), 179–186 (2002).

1. Introduction

The ability of blazed gratings to concentrate almost all of the diffracted energy into a high diffraction order makes them the element of choice when compared to conventional lamellar and sinusoidal gratings. The reason that higher than 1st order grating are not used in the soft x-ray energy range is simply due to the small grazing angles that have to be used to support good reflectivity. To enable the use of high orders therefore, one must have a blazed grating that uses a multilayer coating in order to optimize reflectivity at the blaze condition. Although the multilayer blazed grating (MBG) is an ideal dispersive element, one can also achieve high order diffraction in several other ways. We examine these here briefly so as to show the superiority of the MBG approach.

Firstly one can use lamellar gratings in which the grating structure is etched into a planar multilayer structure [1]. In principle this leads to a convenient manufacturing process in which the multilayer is made in the conventional way, lithography defines the grating pattern, and reactive ion etching etches the grooves. However, a very high aspect ratio of the structure is required to prevent diffraction order overlapping and to direct diffracted energy into one order, as well as achieving a high diffraction efficiency [1–3]. Although very high aspect ratio structures can now be produced by Deep Reactive Ion Etching (DRIE) processes in multilayers [4], it is extremely challenging to meet the high quality required to provide high diffraction efficiency at high order operation of the structure. This is due to the fact that the thickness of the lamellae decreases with increasing order and for reasonable line densities become too thin to be practical in higher orders. The lamellar grating is therefore practically limited to low order operation.

A second possibility is the use of normal incidence blazed transmission gratings such as the Critical Angle Transmission (CAT) grating, in which light is reflected into the blazed wavelength by the internal surfaces of the grating. CAT gratings have demonstrated good efficiency to above the 10th order for a 200 nm period grating, in the soft x-ray energy range [5,6]. The fragile nature of the transmission grating however precludes its use as a monochromatizing element for synchrotron x-ray source applications, due to the 10's of Watts of power the element must absorb due to the quasi broad - band nature of the source. As the dispersive element in a spectrometer, the grating has to be used with collimated light, and so a grazing incidence mirror collimator has to be used, negating the collection aperture advantage of a normal incidence optical element. Further to this, the resolution of a spectrometer is limited by optical aberrations, and the contribution of the entrance and exit slit sizes to the resolution. In a conventional spectrometer, the entrance slit size limited resolution can be expressed as $d\lambda = 1/gm \times ds/r \times \cos\alpha$, where $d\lambda$ is the wavelength resolution, g is the groove density, m is the grating order, ds is the entrance slit or source size, r is the grating to source distance (in the absence of mirror focusing) and α is the angle of incidence. The equivalent expression for the exit slit (or imaging detector pixel size) limited resolution requires use of the exit slit size (ds'), the grating to exit slit distance r', and substitution of β, the angle of diffraction for α. As α is zero for normal incidence, and typically 88 degrees for grazing incidence gratings, the grazing incidence grating can achieve

#221162 - $15.00 USD Received 20 Aug 2014; revised 7 Jan 2015; accepted 20 Jan 2015; published 17 Feb 2015

a resolving power 30 times higher than the normal incidence grating, for the same line density, order and source parameters. In some application areas this advantage is irrelevant, where the source size is effectively zero, such as x-ray astronomy, where objects are point-like and diffraction limited. For synchrotron radiation applications, the source is close and the angular size is relatively large and so the factor of cosα negates the advantages of high groove density and high order operation of the CAT gratings, preventing high resolving power and high throughput. In addition, the number of grooves illuminated has to be at least as high as the resolving power, and while this is easy at grazing incidence, at normal incidence, these membrane gratings would become unreasonably large.

A third possibility is the use of highly asymmetric crystal diffraction [7]. In this method a Bragg diffracting crystal is cut at a large angle with respect to the diffracting planes. The intersection of the Bragg planes with the grating forms a surface grating, and due to the very small periodicity of the grating, the crystal becomes dispersive, with high reflectivity over the Bragg peak. In this case 1st order is used, due to the extreme effective line density of the grating that is formed. While this is a revolutionary concept for hard x-ray spectrometers where silicon crystals can be used, the long wavelength of soft x-rays means that there are no crystals with the right characteristics. The core application wavelength range is from the Oxygen K edge at 2.3 nm wavelength to the Cu $L_{2,3}$ edges at around 1.3 nm wavelength, and therefore crystals with lattice spacing from 1.15 nm to 0.65 nm are required. For the oxygen K edge, only soft organic crystals can be used, and for Cu $L_{2,3}$, natural minerals such as Beryl are the only option. Due to the crystalline defects in both classes of materials, these crystals can only be used for applications requiring a resolving power of typically less than 2000. This type of element is in fact very similar to the MBG as we will show later, but the MBG has the great advantage that in principle it can be made to cover any energy region and can be made highly periodic.

The multilayer blazed grating [8–12] remains therefore as the preferred optical element where very high resolving power is required in the soft x-ray energy region. The widespread use of such elements requires two key developments, the fabrication of nearly perfect multilayers on a grating surface, and a comprehensive understanding of how to optimize the grating parameters in order to achieve high efficiency in high order. The relatively short wavelength implies strict requirements for the quality of the saw-tooth substrates which should have a perfect triangular profile and atomically smooth surfaces of the grooves, and a ML deposition process that should provide perfect replication of the grooves by each of the ML interfaces. Recent progress in fabrication of high quality saw-tooth substrates [13,14] by anisotropic etching of silicon single crystals [15,16] and optimization of the ML growth on such complicated substrates has enabled the demonstration of a diffraction efficiency of approximately 50% for ML-coated blazed gratings (MBG) in the EUV wavelength range [13,14,17–19]. Extension of the MBG technology to the soft x-ray range now seems to be technologically within reach. However, we need to understand how to optimize the performance of the grating in high order, by an optimum choice of the grating parameters, including practical limitations driven by the physical limitations set by material properties and fabrication precision. Understanding the selection of grating parameters that will give optimum higher order performance is the subject of this paper.

This paper is organized as follows. In Sec. 2 the details of simulation are described. In Sec. 3 the data of numerical experiments are presented and discussed. First the dependence of the diffraction efficiency of MBGs on groove density is considered. Thereafter, the impact of diffraction asymmetry on efficiency, refraction, and absorption is investigated. Then examples of optimization of ML parameters are presented. Section 4 summarizes this work.

2. Simulation of high order multilayer grating efficiency

We have approached the problem of simulating MBGs from two directions, firstly using a classical scalar model and secondly using a rigorous electromagnetic model in which

#221162 - $15.00 USD Received 20 Aug 2014; revised 7 Jan 2015; accepted 20 Jan 2015; published 17 Feb 2015

Maxwell's equations are solved for the 2D grating structure. The idea was to check the limits of the validity of the scalar model for these complex gratings, to use this model to define the overall optimization, and for more exact modeling to be done with the full EM simulation. The practical reason for this approach is that direct optimization within the framework of a full EM simulation would be a very time consuming task, and also that use of a scalar model reveals some of the basic physics that defines the performance of the grating.

We first briefly review a simple scalar model of grating efficiency. The blazing effect of blazed gratings is most prominent for the Littrow geometry where incident and diffracted beams are almost normal to the surface of the blazed facets. The geometry is widely used in visible light diffraction gratings (echelle) and was recently demonstrated for a EUV MBG coated with a Mo/Si multilayer which has high reflectance at normal incidence [14,19]. Unfortunately, the Littrow geometry is not relevant for soft x-ray blazed gratings due to the lack of materials having high normal incidence reflectance. The best soft x-ray ML reflectors can provide reflectance as high as 30% at relatively small Bragg angles $\theta \le 10-20^\circ$ [20]. Because of the ML limitations, a soft x-ray MBG must work far from the Littrow geometry with a fairly oblique illumination of the blazed facets. Under these conditions the performance of a blazed grating is affected by shadowing effects [21] and the diffraction efficiency of a blazed order reduces in accordance to the Maystre-Petit phenomenological formula [22]:

$$E_{Maystre} = R \times \min[\cos\alpha / \cos\beta, \cos\beta / \cos\alpha] \quad (1)$$

where R is a reflectance of a blazed facet surface, and α and β are incidence and diffraction angles respectively. The first cosine ratio in the square brackets is chosen for the case of $|\alpha| > |\beta|$, considered in the following [Fig. 1], otherwise the second ratio is relevant. The second term in Eq. (2) is a measure of asymmetry of diffraction; it approaches unity for almost symmetrical diffraction ($|\alpha| \approx |\beta|$) and reduces to zero for the maximal asymmetry ($|\alpha| \to 90^\circ, |\beta| \to 0^\circ$). The asymmetry parameter equals the ratio of the apparent size of the non-shadowed part of a blazed facet surface to the apparent grating period as they are seen at the incidence angle. Only the non-shadowed part of a blazed facet can contribute into a blazed order by "specular" reflection. Shortening of the active part of the blazed facet affects diffraction from an individual groove, resulting in the distribution of energy among a range of angles and hence orders, reducing efficiency in the desired order [21].

According to the Maystre-Petit formula the relative diffraction efficiency, E/R, reduces with the asymmetry and hence with the blaze angle, φ, which couples the angles of incidence, α, and diffraction, β, under the blaze condition via the formula:

$$\alpha = \beta + 2\varphi \quad (2)$$

(In the following we focus our consideration to the grating arrangement shown in Fig. 1, and use absolute values of angles in the Eq. (2) and others). The shadowing effect increases dramatically with blaze angle, where the asymmetry of the diffraction is large. And vice versa, for very small blaze angles the grating efficiency grows, approaching the value of the reflectance of the facet surface. That is why non-Littrow blazed gratings typically have

#221162 - $15.00 USD Received 20 Aug 2014; revised 7 Jan 2015; accepted 20 Jan 2015; published 17 Feb 2015

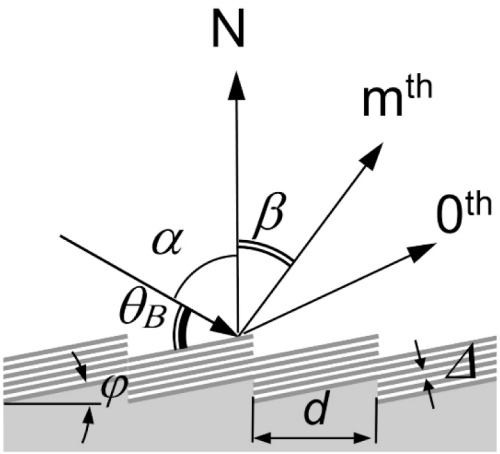

Fig. 1. Diffraction geometry of a multilayer blazed grating: α - angle of incidence, β - diffraction angle for the m^{th} blazed diffraction order, ϕ - blaze angle, θ_B -Bragg angle, d - grating period, Δ - d-spacing of a multilayer, N - normal to the grating plane.

shallow grooves with small blaze angles and work well only in the 1st blazed order, when the asymmetry of diffraction is minimal.

The phenomenological approach for blazed grating efficiency was extended to soft x-rays, and rigorous calculations confirmed that Eq. (1) provided a fairly good prediction of the diffraction efficiency for grazing incidence gratings and MBGs [23–25]. However, these rigorous simulations were performed only for relatively low groove density gratings, which are commonly used in the soft x-ray region due to the limitations described above, while dense gratings were not covered. In this work we present the results of rigorous simulations of diffraction efficiency performed for a wide range of MBG parameters including the grating period and show that the efficiency depends strongly on groove density and can be dramatically improved for ultra-dense gratings as compared to phenomenological predictions.

Simulations of the diffraction efficiency of MBGs were performed using commercial PCGrate codes [26], which are based on the modified boundary integral equation method (MIM) for multilayer gratings [27,28]. The method allows calculation of diffraction from gratings having arbitrary border profiles including random roughnesses and a very small wavelength-to-period (λ / d) ratio, which can present significant difficulties for other rigorous numerical methods. Details of MIM approach for calculation of multilayer coated gratings are published elsewhere [29,30].

All the simulations were performed for wavelengths in the vicinity of the Cu L edge (λ = 1.305 nm) which is relevant for soft x-ray spectroscopy. Most of the MBGs considered in this paper had a W/B_4C coating since this multilayer is one of the best reflectors for soft x-rays at this energy.

Most of the results shown in the paper were obtained for the TE polarization, which is relevant for our synchrotron applications. Unlike in the optical region, in the soft x-ray region polarization effects are not strong at grazing incidence and TM efficiency is similar, typically a few percent lower than the TE efficiency.

Efficiency simulations performed with the MIM approach were cross-checked against other rigorous methods in order to verify the reliability of the results obtained. The diffraction efficiency of a MBG with a period of 200 nm, blaze angle of 6°, coated with 40 W/B_4C bi-layers having a multilayer period Δ of 3.06 nm and Γ-ratio of 0.5 is shown in Fig. 2(a). (The Γ-ratio is the ratio of the thickness of the tungsten layers to the bi-layer d-spacing). The efficiency calculated with MIM and the Generalized Finite Element Method (GFEM) [31,32]

#221162 - $15.00 USD Received 20 Aug 2014; revised 7 Jan 2015; accepted 20 Jan 2015; published 17 Feb 2015

for the 7th blazed order and adjacent orders of the grating demonstrated an excellent agreement.

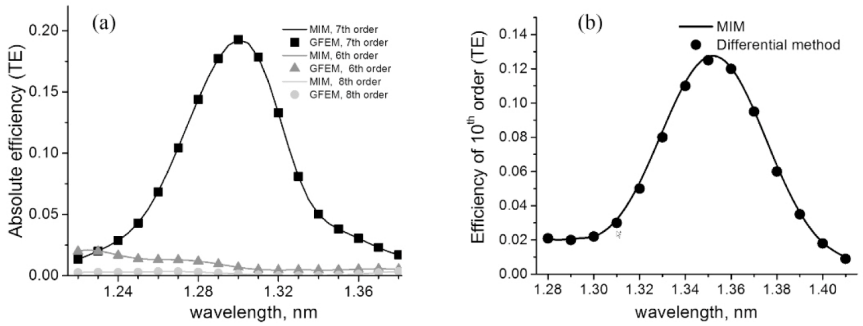

Fig. 2. Diffraction efficiency calculated with MIM and GFEM for a MBG with a period of 200 nm, blaze angle of 6°, 40 W/B_4C bi-layers having a multilayer period Δ of 3.06 nm and Γ-ratio of 0.5 illuminated at an angle of incidence of 83.25°(a). Diffraction efficiency calculated with MIM and the differential method for a MBG with a period of 360 nm, blaze angle of 5°, 30 Rh/C bi-layers having a multilayer period Δ of 3.3 nm and Γ-ratio of 0.33 illuminated with an angle of incidence of 82.8° (b).

Another example of cross-checking is shown in Fig. 2(b), where MIM simulation results are compared to the ones obtained with a rigorous differential approach for a MBG with d = 360 nm, φ = 5°, and blazing in the 10th order, for a MBG coated with 30 pairs of Rh/C layers with thicknesses of 1.089 and 2.211 nm respectively, and optimized for operation at λ = 1.33 nm [Fig. 7 in [23]]. Again good consistency between the two different methods was found.

In summary, the rigorous simulations performed with the MIM approach provide reliable calculations of the high order diffraction efficiency of soft x-ray MBGs.

3. Results and discussion

3.1. Dependence of diffraction efficiency on groove density

We will consider two MBGs which have different periods, d_1 and d_2, with the ratio of the periods an integer number, $k = d_1/d_2$ [Fig. 3]. The gratings have the same blaze angle, φ, and coated with identical multilayers. To provide blazing into the m^{th} diffraction order of a MBG both the grating equation and the Bragg condition should be satisfied, which leads to the formula [8] for the multilayer d-spacing, Δ:

$$\Delta = d \sin\varphi / m, \tag{3}$$

The angle of incidence and diffraction are also the same for both of the gratings. If blazed conditions are satisfied for the m^{th} order of the short-period grating [Fig. 3(b)], the $k \times m^{th}$ order of the long-period grating [Fig. 3(a)] is also under the blazed condition. According to Eq. (1) both the gratings should have the same diffraction efficiency for their respective blazed orders. However, our simulations show that the diffraction efficiency of the blazed orders can differ by a significant factor.

Figure 4 shows efficiency simulation results for two MBGs with a blazed angle of 6° and periods of 200 nm (solid curve) and 800 nm (dashed curve) versus wavelength. The gratings are coated with a W/B_4C multilayer composed of 40 bi-layers with d-spacing of 3.06 nm and Γ-ratio of 0.5. Such a multilayer provides reflectance of 27% (dotted curve) at a Bragg angle of θ = 12.75°. The peak grating efficiency calculated with Eq. (1) for R = 27%, α = 83.25°, and β = 71.25°, is 9.87% as depicted by the star symbol in Fig. 4. The efficiency of the blazed 28th order of the grating with d = 800 nm is 9.2%, in agreement with the prediction of Maystre-Petit equation, while the efficiency of the 7th blazed order of the dense grating with

#221162 - $15.00 USD Received 20 Aug 2014; revised 7 Jan 2015; accepted 20 Jan 2015; published 17 Feb 2015

d = 200 nm reaches 19% and exceeds the phenomenological efficiency by approximately a factor of 2. It

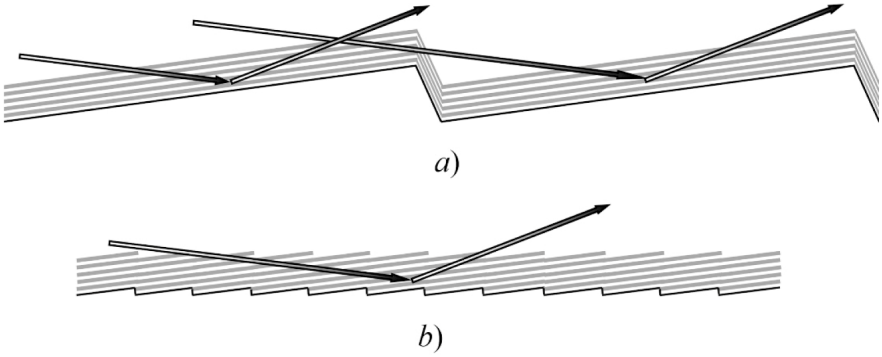

Fig. 3. Schematic of a ML-coated blazed gratings for soft x-rays: (a) a long-period grating with the period larger than an extinction length of the radiation in the multilayer; (b) a short-period grating with the period much smaller than the extinction length. Incident light does not penetrate through the ML stack for the long-period gratings, and the bottom part of the grooves appears to be shadowed. The radiation penetrates through the many semi-transparent grooves of a short-period grating, and therefore a reduction of shadowing is expected.

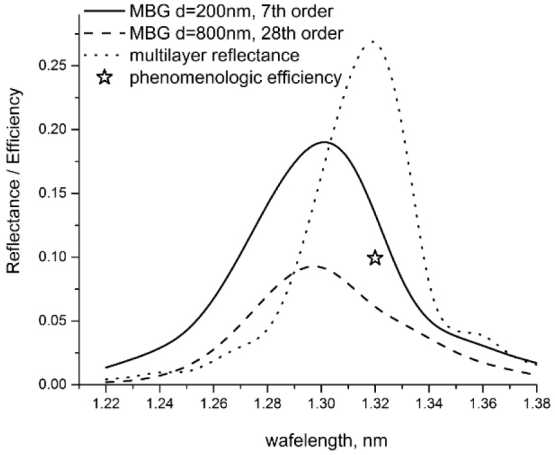

Fig. 4. Calculated TE efficiency of MBGs with periods of 200 nm (solid curve) and 800 nm (dashed curve). The gratings having a blaze angle of 6° are coated with identical W/B_4C multilayers composed of 40 bi-layers with a Δ-spacing of 3.06 nm and Γ-ratio of 0.5. An angle of incidence of 83.25° provides blazed condition for the 7th and 28th diffraction orders of the gratings respectively. Reflectance of the W/B_4C multilayer is shown by a dotted curve. The grating efficiency predicted with the phenomenological approach [Eq. (1)] is depicted by a starred symbol.

should be noted that the MBG peak efficiency is shifted in wavelength with respect to the plane multilayer due to refraction as will be discussed below.

The dependence of the diffraction efficiency on groove density was calculated for a number of blazed gratings with different periods similar to those shown in Fig. 3. The parameters of the gratings are listed in Table 1. All the gratings have a blaze angle of 6° and the same multilayer coating with Δ = 3.06 nm, while the grating period varies over a wide range from 28.6 nm up to 10 μm. The period of the gratings was chosen according Eq. (4) to provide the blaze condition for a defined diffraction order. For example, the 28.6 nm grating has the 1st order under the blaze condition, while the 200 nm and 10 μm gratings are optimized for the 7th and 350th blazed order respectively (Table 1). Angles of incidence and

#221162 - $15.00 USD Received 20 Aug 2014; revised 7 Jan 2015; accepted 20 Jan 2015; published 17 Feb 2015

diffraction are the same for all the gratings. The identical geometry of diffraction allows investigation of solely the impact of groove density on MBG efficiency.

The efficiency of the MBGs having different periods is shown in Fig. 5. The data demonstrate that soft x-ray blazed gratings can deliver high efficiency in a very high diffraction order, similarly to those used in visible light. For example, a grating with a period of 1 μm has an efficiency of about 10% in the 35th order, and the grating with a period of 10 μm demonstrates the same efficiency in the 350th diffraction order. Such a high order operation in the soft x-rays is not practical for traditional reflection gratings due to the grazing angle limitations. Grazing incidence gratings can operate only at very oblique illumination at the glancing angles smaller than the critical angle for total external reflection from a facet surface. This limits the blaze angle to small values, and hence can provide blazed conditions only for the 1st diffraction order. A MBG can operate at much larger blaze angles due to its ML coating, and hence can direct energy into a very high diffraction order with high efficiency. Moreover, the non-grazing incidence geometry of a MBG mitigates shadowing effects as compared to a grazing incidence blazed gratings having the same groove profile (i.e. the same period and the same blaze angle). While using a grazing geometry the angles of incidence and diffraction are close to 90° and shadowing is maximal, the shadowing is relaxed for a blazed grating due to the smaller values of α and β.

Table 1. The period and the corresponding blazed orders for the ML blazed gratings used for efficiency simulations shown in Fig. 5. All other parameters are the same for all the gratings: the blaze angle of 6°, the incident angle of 83.25°, a W/B_4C multilayer with a Δ-spacing of 3.06 nm, a Γ-ratio of 0.5, and the number of bi-layers is 40.

Grating period *d*, nm	28.6	57.1	85.7	114.3	142.9	200	400	600	800	1000	2000	5000	10000
Number of a blazed order *m*	1st	2nd	3rd	4th	5th	7th	14th	21st	28th	35th	70th	175th	350th

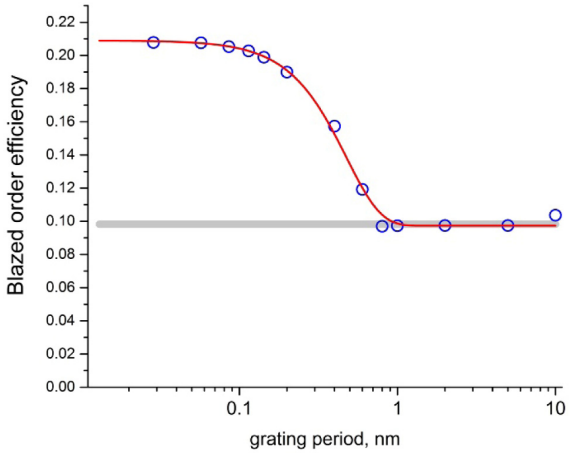

Fig. 5. Dependence of the efficiency of W/B_4C blazed gratings coated by 40 bi-layers on the grating period (circles). All the gratings have the same blaze angle of 6°, identical ML coating, and the same incidence angle of 83.25°. The efficiency calculated with the phenomenological approach is depicted with a grey line. The red curve is a fit of the efficiency data with the modified phenomenological function (4).

The efficiency of MBGs with relatively low groove density is consistent with the phenomenological Maystre-Petit formula (1), i.e. it is determined by the ML reflectance and shadowing effects. For the case shown in Fig. 4, with a ML reflectance of 26.8% and a geometry factor of $\cos 83.25^\circ / \cos 71.25^\circ = 0.37$ the phenomenological efficiency (the grey

#221162 - $15.00 USD Received 20 Aug 2014; revised 7 Jan 2015; accepted 20 Jan 2015; published 17 Feb 2015

line in Fig. 5) should not exceed 10% for all the gratings listed in Table 1. However, our simulations reveal a pronounced effect of the groove density on the diffraction efficiency of MBGs. An increase in the groove density of a MBG results in a large efficiency gain. As soon as the grating period becomes shorter than 1 μm the efficiency increases and eventually exceeds the phenomenological prediction more than a factor of 2 for gratings with periods of 200 nm or less [Fig. 5].

The dependence of the diffraction efficiency of MBGs on period, d, of a grating demonstrates a threshold behavior [Fig. 5], while the Maystre-Petit formula (1) assumes no dependence of the efficiency on groove density. We find that the dependence of diffraction efficiency on grating period at fixed α, β, and λ is well described with an empirical formula:

$$E = R_0 \left\{ \cos\alpha / \cos\beta + A\exp[-(d/L)^2] \right\} \quad (4)$$

where A is the maximum additional increase in the efficiency for ultra-dense MBGs, and the parameter L has the physical meaning of an attenuation length for soft x-rays in the multilayer. The Eq. (4) is a modification to the Maystre-Petit model which takes into account groove transmission. The first term in the square brackets is the Maystre-Petit geometry factor which as we mentioned above represents the non-shadowed part of a groove, while the second term describes the contribution of the semi-shadowed part of the grooves to the net diffraction efficiency. The exponential term in Eq. (4) gives the dependence of the efficiency gain on groove density. When the period of a MBG is much shorter than the attenuation length, the extra efficiency caused by groove transparency is maximal and is equal to A. (A physical meaning of the parameter A and dependence of A and L on asymmetry of diffraction will be discussed below in the section 3.2.). When the MBG period is equal to the attenuation length, which was estimated as L = 470 nm by fitting the efficiency data shown in Fig. 5 with Eq. (4), the effect of groove transparency reduces by a factor of 1/e, since only a small portion of the x-rays reaches the semi-shadowed part of the groove downstream. The groove transparency goes down to zero when the grating period approaches 1 μm as seen in Fig. 5. This is consistent with the distance the soft x-rays penetrate into a W/B_4C multilayer of semi-infinite thickness, which can be estimated from the dependence of the multilayer reflectance on the number of bi-layers. The reflectance increases with the number of bi-layers, N, and saturates at $N \approx 70$ [20]. That means that (W/B_4C)70 multilayer is not transparent at the wavelength of 1.3 nm at the Bragg angle of 12.75°, and the x-rays are attenuated almost completely at a distance of 3.06 nm × 70 / sin 12.75° = 970 nm. The non-transparent 1 micron long grooves of the MBG cause maximum possible shadowing of neighboring grooves and efficiency reduces down to the value predicted by the Maystre-Petit formula (1). Based on these considerations a rule of thumb for the design of highly efficient MBGs can be formulated as follows: the grating grooves separation should be so short that the x-rays when passing from one groove to another intersect a number of bi-layers much smaller than required for saturation of the multilayer reflectance. From simple geometry considerations, an equivalent formulation of the rule is: the height of the grating grooves should be much smaller than the thickness of the multilayer with saturated reflectance. Note the minimal possible groove height equals to one bi-layer spacing. This however requires a saw-tooth substrate with extremely short grooves, which is a significant technological challenge. On the other hand, high quality gratings with a period of 100-200 nm can be successfully fabricated as has been demonstrated [13,14] and Fig. 5 shows that the efficiency of such gratings can be as high as for ultra-dense gratings with the period of 28.6 nm. This makes dense high-order gratings the most promising candidate for practical applications in the nearest future.

Equation (5) shows a few ways to improve the diffraction efficiency of MBGs. One can use less absorbing multilayers with longer L, which can be realized by a reduction of the Γ-ratio and use of lower Z materials for the absorber layer of a ML stack. This, however, has an obvious restrictions because the choice of soft x-rays materials is limited, and reduction of the

#221162 - $15.00 USD Received 20 Aug 2014; revised 7 Jan 2015; accepted 20 Jan 2015; published 17 Feb 2015

Γ-ratio far below an optimal value [33,34] will result in reduction of ML reflectance. The second approach is to increase the groove density to have grating periods much shorter than an attenuation length. Given the recent advancements in short period grating fabrication techniques, this seems like a very promising direction. The third approach is to increase the value of the extra efficiency parameter A for ultra-dense MBGs. The latter requires careful optimization of MBG design and geometry of diffraction as will be shown in the next section.

In summary, soft x-ray MBGs have a great advantage over grazing incidence gratings due to the fact that they are capable of providing high diffraction efficiency in a high diffraction order. We discovered that diffraction efficiency depends strongly on the groove density and ultra-dense MBGs demonstrate unique efficiency characteristics in the soft x-ray spectral region. As soon as the grating period becomes shorter than the attenuation length of the radiation in the multilayer, the transparency of the grooves increases and shadowing effects are minimized, resulting in a remarkable increase in diffraction efficiency. One can obtain at least a two-fold enhancement of efficiency in a defined blazed order by a proper choice of the grating period value.

3.2. Relative efficiency of dense MBGs: dependence on asymmetry of diffraction

In the previous section we found that diffraction efficiency of a dense MBG can be much higher than that of a traditional low groove density grating. However, even for ultra-dense MBGs efficiency remained lower than the ML reflectance, and maximum relative efficiency, E/R, did not exceed 0.78 [see Fig. 4 and Fig. 5]. This result was obtained for a particular geometry of diffraction defined by the asymmetry parameter value $\cos\alpha / \cos\beta = 0.37$. In this section we will investigate diffraction efficiency of ultra-dense MBGs for a wide range of the asymmetry parameters.

To explore the impact of the asymmetry on diffraction efficiency, we consider 3 dense MBGs coated with identical multilayers, but optimized for different blazed orders. The gratings have the same period d = 200 nm, but different blaze angles of 0.86°, 6°, and 7.72°, calculated using Eq. (3), which provided blazing for the 1st, 7th, and 9th diffraction orders respectively (Table 2). All the gratings were coated with (W/B_4C)40 multilayers with d-spacing of 2.99 nm and Γ-ratio of 0.5. The angle of incidence on the gratings was calculated for each grating using the equation [see Fig. 1]:

$$\alpha + \theta = 90° + \varphi, \tag{5}$$

to keep the Bragg angle θ = 12.75° the same for all the gratings. Under these conditions the reflectance of the multilayer stack under a simple scalar model would be the same for all the gratings, which allows the investigation of the dependence of the diffraction efficiency solely on the asymmetry of diffraction. The simulation results shown in Fig. 6 reveal a few prominent trends which are enhanced with asymmetry: reduction of diffraction efficiency, as well as a shift and width change of the efficiency curves. The efficiency curves are shifted towards shorter wavelengths as compared to the reflectance curve of the ML, and the shift increases with the asymmetry of diffraction. At the same time a substantial broadening of the efficiency curves occurs. The direction of the shift and the sign of the width changes depend, however, on the geometry of diffraction and are opposite for positive and negative blazed orders. The latter is illustrated in Fig. 7 for a MBG with the period of 200 nm, blaze angle of 7.12°, and coated with a W/B_4C multilayer with 51 bi-layers, a Δ-spacing of 2.75 nm and a Γ-ratio of 0.2. Here solid black and grey curves depict the efficiency of the 9th positive and 9th negative orders of the MBG respectively, and the ML reflectance is shown with a dashed curve. The incidence

#221162 - $15.00 USD Received 20 Aug 2014; revised 7 Jan 2015; accepted 20 Jan 2015; published 17 Feb 2015

Table 2. Parameters of the MBGs optimized for the 1st, 7th, and 9th blazed orders. All the gratings have a period of 200 nm, and are coated with the same W/B_4C multilayer with 40 bi-layers, a Δ-spacing of 2.99 nm and Γ-ratio of 0.5.

Blaze angle φ, °	Number of a blazed order m	Angle of incidence α, °	Asymmetry parameter, b	λ_{max} from Fig. 6, nm	λ_{max} from Eqs. (7) - (9), nm
0.86	1	78.11	–0.876	1.286	1.286
6	7	83.25	–0.366	1.260	1.264
7.72	9	84.97	–0.251	1.240	1.246

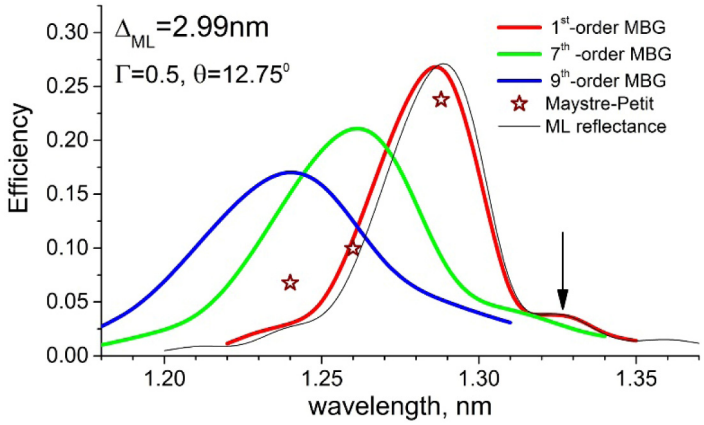

Fig. 6. Diffraction efficiency of the MBGs optimized for the 1st, 7th, and 9th blazed orders (see Table 2). All the gratings have a period of 200 nm, and are coated with the same W/B_4C multilayer with Δ-spacing of 2.99 nm and Γ-ratio of 0.5, so that a Bragg angle of 12.75° was kept in all the cases. The arrow depicts a resonant wavelength calculated with no refraction taken into account.

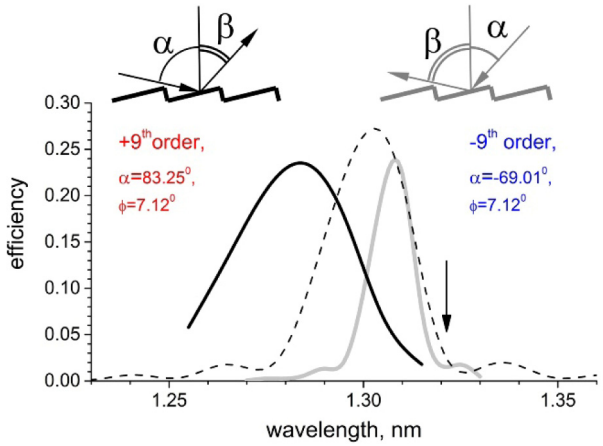

Fig. 7. Efficiency of the positive 9th blazed order of a ML coated blazed grating (black solid curve) and the negative 9th blazed order (gray solid curve). The efficiency curves are shifted in opposite directions with respect to the ML reflectance curve (dashed curve) which corresponds to the case of symmetrical Bragg diffraction. The grating has a period of 200 nm, blaze angle of 7.12°, and is coated with a W/B4C multilayer with 51 bi-layers, a Δ-spacing of 2.75 nm and a Γ-ratio of 0.2.

angles were 83.25° and 69.01° for the positive and negative order diffraction respectively to provide the same Bragg angle as for the flat multilayer. While the efficiency curve of the positive blazed orders shift towards shorter wavelengths and become wider, it moves towards longer wavelengths and becomes narrower for the negative order diffraction geometry.

#221162 - $15.00 USD Received 20 Aug 2014; revised 7 Jan 2015; accepted 20 Jan 2015; published 17 Feb 2015

The change of position and width of the efficiency curves can be explained with the dynamical theory of x-ray diffraction for asymmetrically cut single crystals [35]. We assume here generic similarity between the MBGs and asymmetrical crystals. Indeed, while conventional flat multilayers are in fact artificial one-dimension crystals with "Bragg planes" parallel to the "crystal" surface, a MBG [Fig. 3(b)] has essentially the same structure as an asymmetrical crystal with Bragg planes tilted at an angle with respect to the crystal/grating surface. Diffraction in both cases should follow the same pattern, and the predictions of the dynamical theory of asymmetric x-ray Bragg diffraction can be applied for analysis of the diffraction of MBGs.

According to dynamical theory for symmetric diffraction, Bragg's law includes a refraction correction term, ω_s:

$$2\Delta \sin\theta = n\lambda(1+\omega_s), \tag{6}$$

which results in some shift of the resonance wavelength for symmetrical crystals or flat multilayers towards shorter wavelengths. An arrow in Fig. 6 depicts the position of the ML reflectance curve for the kinematic approximation in the absence of refraction ($\omega_s = 0$). In the case of asymmetrical diffraction the refraction correction term, ω_a, is somewhat different from the one for the symmetrical case, ω_s,

$$\omega_a = \omega_s(b-1)/(2b), \tag{7}$$

and the difference depends on the asymmetry parameter, b:

$$b = \sin(-\theta \pm \varphi)/\sin(\theta \pm \varphi) \tag{8}$$

where signs '+/–' correspond to direct ($\alpha>\beta$), or reciprocal ($\alpha<\beta$) diffraction geometry. The asymmetry parameter is similar to the Maystre-Petit factor (compare b to the term in square brackets in Eq. (1)). The main difference is that the Maystre-Petit factor has the same value for a direct and reciprocal geometry while b is different. When a cut angle, φ, of a crystal (or blaze angle of an MBG) equals zero, the asymmetry parameter is $b = -1$, corresponding to symmetrical Bragg diffraction, and $\omega_a = \omega_s$. As the blaze angle increases, the parameter b deviates from -1, and the refraction term differs from the one (see Table 2) for the symmetrical case, $\omega_a \neq \omega_s$. As a result, the resonance Bragg wavelength shifts with respect to the symmetrical one. The shift increases with blaze angle as larger blaze angles result in higher asymmetry (see Eq. (8)). In this way the MBGs optimized for different blaze orders give different positions of the efficiency curves [Fig. 6]. The shift of position of the maxima in the efficiency curves is in good agreement with the one predicted by Eqs. (6)-(8) as shown in Table 2.

Since the asymmetry parameter, b, is different for direct and reciprocal diffraction geometry, the asymmetrical refraction term, ω_a, can be larger or smaller than the symmetrical one, ω_s, depending on the geometry. For the grating shown in Fig. 7 the asymmetry parameter equals -0.328 and -3.047 for direct and reciprocal geometry respectively. As a result, the efficiency curves shift towards shorter wavelengths for the direct geometry, and towards longer wavelengths for the reciprocal geometry [Fig. 7].

The dynamical theory also explains observed changes of the shape of the efficiency curves. According to the theory, the spectral width of total Bragg reflection depends on the asymmetry as:

$$(\lambda/\Delta\lambda)_a = \sqrt{|b|}(\lambda/\Delta\lambda)_s \tag{9}$$

which means broadening and narrowing of spectral width for the direct and reciprocal geometry respectively.

#221162 - $15.00 USD Received 20 Aug 2014; revised 7 Jan 2015; accepted 20 Jan 2015; published 17 Feb 2015

The efficiency of the MBGs shown in Fig. 6 is much higher than the phenomenological approach predicts (star symbols in Fig. 6), especially for high blazed orders. For example, the 9th blaze order grating demonstrates efficiency as high as 17% which exceeds the 6.8% calculated with Eq. (1) by a factor of 2.5. Nevertheless the diffraction efficiency is lower than the ML reflectance and the difference increases with the asymmetry. The relative efficiency of the grating optimized for the 1st blazed order is almost 1, but it reduces down to 0.63 for the 9th-order MBG.

One can expect further reduction of efficiency for more asymmetrical diffraction conditions. To explore the efficiency behavior in a wide range of the asymmetry parameter including highly asymmetrical cases we used ultra-dense 1st order gratings (Table 3). All the gratings are coated with the same multilayer, while the grating period was chosen according the Eq. (3) to provide the blazing condition for the 1st diffraction order. Such gratings have the highest possible diffraction efficiency since they have the shortest possible periods and impact of the exponential term in Eq. (4) on diffraction efficiency is minimal for these gratings. The dependence of the relative efficiency on asymmetry is shown in Fig. 8 by symbols, the scalar efficiency calculated using the Eq. (1) is shown with a green line for comparison. The efficiency of the ultra-dense MBGs exceeds the scalar efficiency in the

Table 3. Parameters of 1st-order MBDs for relative efficiency calculations summarized in Fig. 8.

Grating period, nm	Blaze angle, deg.	Angle of incidence, deg.	cosα/cosβ	Relative efficiency	Multilayer parameters			
					Materials	d-spacing	Γ-ratio	Number of bi-layers
87.64	2	79.25	0.733	0.985				
43.85	4	81.25	0.528	0.943				
31.91	5.5	82.75	0.403	0.876	W/B_4C	3.06	0.5	40
25.10	7	84.25	0.296	0.772				
21.98	8	85.25	0.234	0.669				
19.55	9	86.25	0.177	0.478				

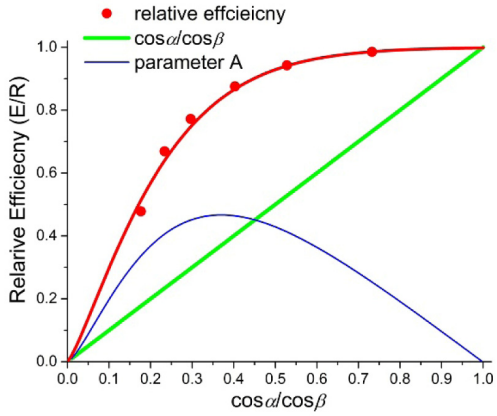

Fig. 8. Dependence of relative diffraction efficiency on diffraction asymmetry (solid symbols and red line), calculated for ultra-dense MBGs listed in Table 3. The multilayer parameters (d-spacing, Γ-ratio, Bragg angle etc.) are the same for all the gratings. The diffraction efficiency exceeds the one calculated with the Maystre-Petit formula (green line). The dependence of parameter *A* from Eq. (4), which is a difference between the two calculations, is shown with a blue curve.

whole range of the asymmetry parameter. For example, while scalar efficiency reduces down to 0.4 for $\cos\alpha / \cos\beta = 0.4$, the real efficiency of the ultra-dense grating remains as high as 0.9 exceeding the scalar value more than by a factor of 2. The difference between the scalar and

#221162 - $15.00 USD Received 20 Aug 2014; revised 7 Jan 2015; accepted 20 Jan 2015; published 17 Feb 2015

real efficiencies corresponds to the parameter A in the Eq. (4), which is shown with a blue curve.

We found, however, that dependence of the relative efficiency on the asymmetry parameter, shown in Fig. 8 with a red curve is not universal. The same value of a $\cos\alpha / \cos\beta$ ratio can be realized for a variety of combinations of α and β, and diffraction efficiency can be significantly different for those cases. Nevertheless the general trend of reduction of efficiency with the asymmetry was observed for all our simulations.

We found that reduction of efficiency with the asymmetry is accompanied with enhanced absorption of x-rays under asymmetrical conditions. To probe the dependence of absorption and transmission of the ML stack on the asymmetry we assumed that a saw-tooth substrate is absolutely transparent and coated with a semi-transparent W/B_4C multilayer composed of only 25 bi-layers (Table 4), while about 40 layers are necessary for ML reflectance saturation which corresponds to zero transparence. In this way we can calculate not only diffraction efficiency but also transmitted energy and absorption inside the ML stack. The results of the simulations shown in Fig. 9(a) reveal enhanced absorption in the MBGs, which increases from 0.62 for the flat multilayer ($\cos\alpha / \cos\beta = 1$) to 0.8 for the highest asymmetry ($\cos\alpha / \cos\beta = 0.25$) considered here. At the same time the transparency of the 25-bilayer multilayer stack reduces from 0.16 to almost zero.

Table 4. Absolute efficiency of the 1st blaze order MBGs with different blazed angles. All the gratings are coated with W/B_4C multilayers composed of 25 bi-layers with d-spacing of 2.99 nm and Γ-ratio of 0.5.

Grating period, nm	Blaze angle, deg.	Angle of incidence, deg.	cosα/cosβ	Absolute efficiency
22.22	7.72	84.9736	0.25332	0.1611
28.57	6	83.25	0.3727	0.1863
52.9	3.24	80.486	0.60572	0.21019
200	0.86	78.10561	0.88226	0.21
200	0	77.25	1	0.21393

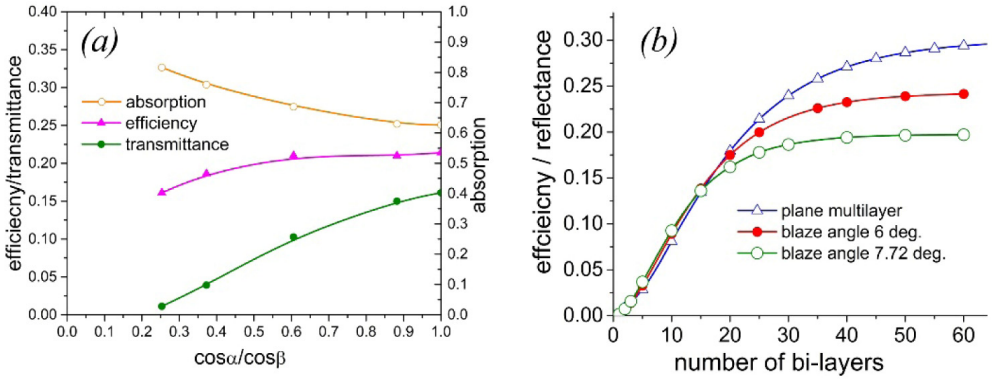

Fig. 9. (a) Transmitted energy (circles), absorbed energy (open circles), and absolute efficiency (triangles) for the MBG gratings with different blaze angles listed in the Table 4. (b) Dependences of diffraction efficiency on the number of bi-layers for the gratings with a blaze angle of 6° and 7.72° (see Table 4) are shown by curves with solid and open circles respectively; reflectance of the respective plane multilayer versus the number of bi-layers is shown with a curve with triangle symbols.

Due to enhanced absorption and reduced transparency of a ML stack under asymmetrical diffraction, the penetration length of x-rays is much shorter and one can expect efficiency saturation to occur at a smaller number of the bi-layers as compared to symmetrical Bragg diffraction. Indeed, we found that the efficiency of blazed gratings saturates at a much smaller number of bi-layers than the reflectance of plane multilayers [Fig. 9(b)]. While 45 bi-layers are required to obtain reflectance of 0.95 from the saturated value for the W/B_4C multilayer, only 38 and 31 bi-layers are enough to achieve efficiency of 0.95 from the saturated values

#221162 - $15.00 USD Received 20 Aug 2014; revised 7 Jan 2015; accepted 20 Jan 2015; published 17 Feb 2015

for the MBGs with the blaze angles of 6° and 7.72° respectively. The fact that a highly asymmetrical MBG requires a much thinner coating is very important from a technological point of view. Thinner coatings are preferable because a ML trends to smooth out the saw-tooth grooves which has a negative impact on the grating efficiency [13], and the smoothing increases with the coating thickness [36].

The observed growth of absorption and reduction of efficiency with asymmetry should be investigated in detail using rigorous dynamical theory. A full theoretical analysis of this aspect is beyond the scope of this paper. We just point out two obvious factors which can affect absorption and efficiency of MBGs. First, an absorption path is always longer for asymmetrical diffraction as can be seen from simple geometrical considerations [Fig. 10]. Indeed, a path L, for light passing through a multilayer when reflected from an interface buried at a depth, h, for the symmetrical case is $L_s = 2h / \sin\theta$, while for the asymmetrical case the path is $L_a = h(\sin^{-1}(\theta - \varphi) + \sin^{-1}(\theta + \varphi))$. The absorption length L_a has a minimum value at the $\varphi = 0$, which corresponds to the symmetrical case, and increases with the blaze angle, causing stronger absorption of the radiation within the multilayer. In other words the same multilayer has different absorption in symmetrical and asymmetrical geometry. Since the absorption path is always longer for asymmetric geometry, $L_a > L_s$, the efficiency of a MBG is always smaller than the ML reflectance.

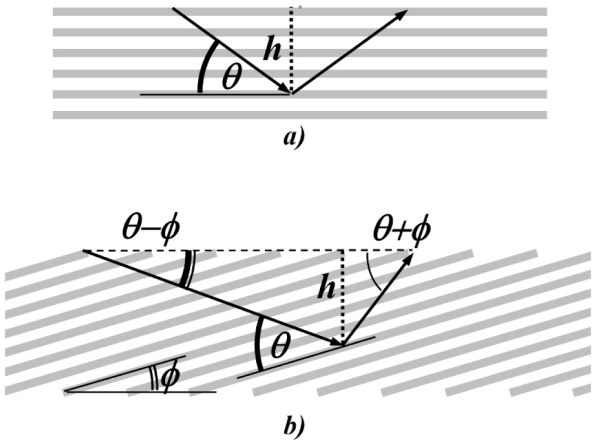

Fig. 10. Schematic of symmetric (a) and asymmetric (b) Bragg diffraction. Arrows show the path of soft x-rays reflected from an interface buried at the depth h in a multilayer. Since the absorption length is always longer for asymmetrical diffraction, absorption is always stronger for a MBG as compared to a correspondent flat ML.

The second factor affecting diffraction efficiency is refraction effects which result in a shift of the efficiency curves in Fig. 6 and Fig. 7. A shift in the efficiency maxima with respect to the ML reflectance means that the blazed wavelength is different from the resonant wavelength of the multilayer. This alters the blazing condition (3) which assumes that a diffracted beam of maximum efficiency goes in the direction of specular reflection of the incident beam from the facet surface. The maximum efficiency of a MBG is observed for the direction which corresponds to a diffraction angle for the blazed wavelength which varies with the asymmetry [Fig. 6 and Fig. 7]. That means that an effective blaze angle of a MBG is somewhat different from the geometrical blaze angle defined as a slope angle of the blazed facets. Our simulations show that difference between effective blaze angle and blazed facet slope increases with the asymmetry and this correlates with reduction of diffraction efficiency [Fig. 11]. Due to deviation from the condition of exact specular reflection of x-rays from the ML interfaces the blazing is partially compromised. The effect is probably similar to an offset from the exact Bragg condition in crystals, which results in a perturbation of an ideal standing

#221162 - $15.00 USD Received 20 Aug 2014; revised 7 Jan 2015; accepted 20 Jan 2015; published 17 Feb 2015

wave. In the case of maximum efficiency, the antinodes are located in positions of minimum electron density [37], but in the detuned case, the antinode shift into higher electron density regions, resulting in an increase in absorption. All these factors lead to reduction of diffraction efficiency.

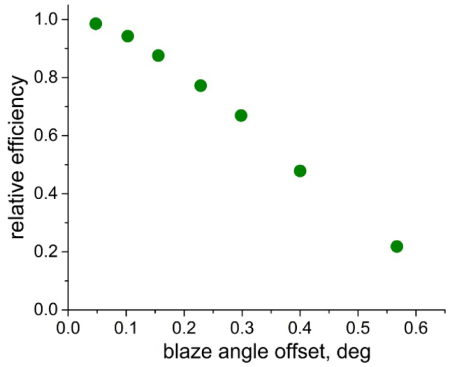

Fig. 11. Relative diffraction efficiency of the MBGs listed in Table 3 versus offset of the effective blaze angle from the "geometrical" blaze angle.

Since the blaze angle offset is caused by refraction, taking into account refraction effects is one of the key points in optimization of the grating efficiency. For example, one should avoid small grazing angles of incidence (or diffraction) since such geometry results in stronger refraction [33,34] and eventually low efficiency. This might be challenging because shallow illumination/diffraction is often necessary for high dispersion and resolving power required for RIXS spectroscopy. In this case one should consider alternative ways of achieving high dispersion such as an increase of groove density or high order operation [38].

As we mentioned above, ultra-dense MBGs look similar to asymmetrical Bragg crystals. There is an even more obvious similarity between MBG and ML-sliced gratings which are fabricated by an oblique cut of a ML deposited on a flat substrate [39]. Indeed, sliced gratings are essentially a 1st order blazed grating, and the structure of a multilayer stack of the MBG shown in Fig. 3(b) is essentially identical to a sliced multilayer. This connection is supported by efficiency calculations which show that similar to MBGs, the sliced grating demonstrates a very high efficiency, and can approach the ML reflectance [40].

In summary, we found that the efficiency of MBGs depends on the asymmetry of diffraction. Diffraction asymmetry causes refraction effects such as a shift of the resonance wavelength, a change of the spectral bandwidth, absorption enhancement, weakening of blazing ability, and eventually results in reduction of diffraction efficiency. The refraction effects can be well predicted by dynamic theory for asymmetrical Bragg diffraction. Optimization of design of a grating and a whole spectrometer should aim at finding an optimal diffraction geometry to balance efficiency and resolution requirements.

3.3. Absolute efficiency of dense MBGs: multilayer optimization

In the previous section we found that the diffraction efficiency of ultra-dense MBGs is strongly affected by refraction phenomena. Under the condition of strong asymmetry of diffraction which is desirable for high spectral resolution, the refraction can result in significant reduction of the efficiency. Fortunately since MLs are artificial media they offer possibilities to control refraction by optimization of the ML parameters. For example, absorption and refraction of soft x-rays in a multilayer can be reduced by shrinking the Γ-ratio and/or by choice of less absorbing materials of the ML. In addition, use of reasonably small d-spacing MLs allows operation at larger Bragg angles, θ, which reduces the asymmetry for a fixed blaze angle (see Eqs. (5), (7), and (8)), and hence mitigates absorption and refraction.

#221162 - $15.00 USD Received 20 Aug 2014; revised 7 Jan 2015; accepted 20 Jan 2015; published 17 Feb 2015

The optimization should be performed for each particular case in terms of requirements and constraints of a whole spectrometer design. In this section we will give an example showing that a proper choice of a multilayer can significantly mitigate the negative impact of asymmetry and improve absolute efficiency.

To investigate the impact of ML parameters on MBG's performances, we consider four identical gratings with a period of 200 nm and a blaze angle of 7.12°, but coated with multilayers having different absorbing and refractive characteristics. The parameters of the gratings and multilayers are listed in Table 5. The values of ML d-spacing, Bragg angle, and angle of incidence were calculated using Eqs. (2) and (4) to provide blazed conditions for the 9th diffraction order of the gratings. Absorption and refraction of the multilayers for the gratings #1-#4 were successively reduced by increasing the Bragg angle (gratings #2 versus #1), by reduction of Γ-ratio (gratings #3 versus #2), and by replacement of the Tungsten layers by Molybdenum ones (grating #4 versus #3). Such a variation of the ML parameters results in a progressive shift of the ML reflectance curves to longer wavelengths and towards the resonance wavelength value calculated for zero refraction [Fig. 12]. Since less absorbing multilayers require more bi-layers to have a certain reflectance, the number of bi-layers was adjusted accordingly to provide the same reflectance for all the ML coatings [Fig. 12]. In this way the ML reflectance is the same for all the MBGs, and the impact of ML parameters on MBG diffraction efficiency can be investigated in isolation.

The results of the efficiency simulation for the gratings #1 to #4 demonstrate the importance of ML parameter optimization for MBG efficiency [Fig. 13]. Use of a short-period ML results in a smaller asymmetry of diffraction due to larger Bragg angles and improves diffraction efficiency (b = –0.266 for the gratings #1 and b = - 0.328 for the grating #2, see Table 5). Further improvement of diffraction efficiency can be achieved by replacement of the multilayer #2 with a less absorbing one #3 with smaller Γ-ratio. Reduction of the multilayer Γ-ratio from 0.5 to 0.2 (gratings #2 and #3) reduces the shift and improves efficiency of the 9th order up to 23.5%. Note, that the 9th order efficiency value is close to the ML reflectance of 27.2% [see Fig. 13], and exceeds the one calculated with the Maystre-Petit formula by a factor of 2.5. This example demonstrates that with the optimal choice of parameters, a ML can provide remarkable efficiency in a high diffraction order for an ultra-dense MBG. That means that spectral resolution can be improved due to high-order operation of the grating by a factor of 9 in this case with minor efficiency losses over a 1st order grating.

One could expect additional improvement of efficiency with further reduction of ML absorption. However, replacement of the W/B_4C multilayer with a less absorbing Mo/B_4C multilayer (gratings #3 and #4) results in some reduction of the efficiency [Fig. 13]. This is probably related to the fact that asymmetry affects the saturation of multilayers [see Fig. 8(b)]. Both the multilayers #3 and #4 are under-saturated since saturation occurs at approximately 80 and 120 bi-layers for W/B_4C and Mo/B_4C respectively [20]. Under conditions of asymmetrical diffraction, the multilayers become more saturated since a lower number of bi-layers is required for the saturation [see Fig. 8(c)]. Since saturated W/B_4C has higher reflectance than Mo/B_4C [20], the W/B_4C-coated grating is more efficient.

Table 5. Parameters of the 200 nm blazed gratings with a blaze angle of 7.12° coated with multilayers having different refractive properties. The average refraction index of the multilayers reduces progressively for the gratings #1 to #4.

Grating / ML	Angle of incidence α,	Multilayer parameters					Asymmetry parameter, b
		Materials	d-spacing, nm	Γ-ratio	Number of bi-layers N	Bragg angle θ,	
#1	84.97	W/B_4C	2.987	0.5	40	12.75	–0.283
#2	83.25	W/B_4C	2.754	0.5	50	13.87	–0.328
#3	83.25	W/B_4C	2.754	0.2	51	13.87	–0.328
#4	83.25	Mo/B_4C	2.754	0.2	83	13.87	–0.328

#221162 - $15.00 USD Received 20 Aug 2014; revised 7 Jan 2015; accepted 20 Jan 2015; published 17 Feb 2015

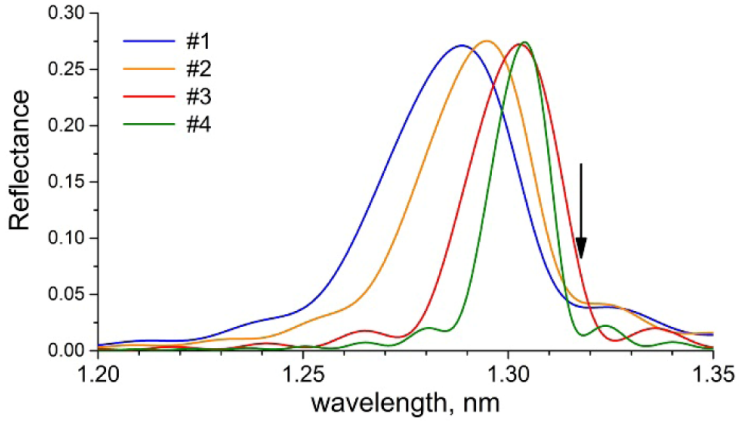

Fig. 12. Reflectance of the MLs used in simulation of different MBGs listed in Table 5. The ML parameters listed in Table 5 were varied so that the average refraction index of the multilayers reduces progressively. As a result, the reflectance curves shift gradually towards longer wavelengths. The number of bi-layers was adjusted for each ML in order to obtain the same reflectance for all of the MLs.

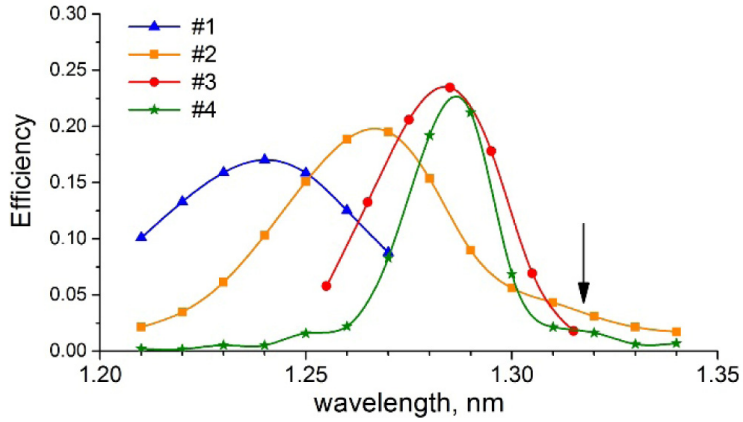

Fig. 13. Efficiency of the 9th diffraction order of 200 nm period blazed gratings #1-#4 with a blaze angle of 7.12°, as listed in Table 5, coated with the multilayers shown in Fig. 9. The parameters of the gratings and the MLs were varied to investigate the dependence of MBG diffraction efficiency on ML d-spacing (the gratings #1 and #2), ML Γ-ratio (the gratings #2 and #3), and ML materials (the gratings #3 and #4).

In summary, the choice of ML parameters for a MBG is complex and here we have developed generally applicable guidelines for optimization. The ML design optimization should be done in terms of refraction and reflectance saturation effects dependent on the diffraction asymmetry.

4. Summary

The performance of soft x-ray MBGs depends strongly on the parameters of the saw-tooth substrates and the multilayer. Grating groove density is one of the crucial MBG's parameters which dramatically affect grating efficiency. Ultra-dense MBGs have superior characteristics as compared to low groove density gratings which are traditionally used in soft x-ray instrumentation. When the period of a MBG is shorter than an attenuation length for soft x-rays, the multilayer grooves of the grating become semi-transparent. This reduces the shadowing effect which causes efficiency loss and results in efficiency gain. Ultra-dense

#221162 - $15.00 USD Received 20 Aug 2014; revised 7 Jan 2015; accepted 20 Jan 2015; published 17 Feb 2015

MBGs can exhibit two-fold or more efficiency improvement as compared to the efficiency of traditional low groove density gratings, limited by the Maystre-Petit factor.

Another important parameter is the asymmetry of the diffraction geometry of a MBG which should be carefully considered in optimization of a grating and a complete spectrometer. Refraction effects caused by the asymmetry result in changes in the blazed wavelength and in the effective blaze angle of a MBG, compromising the blazing ability of the grating and eventually leads to a reduction of diffraction efficiency. Dynamic theory of diffraction for asymmetrically cut crystals was found to predict refraction effects in MBGs very well.

A proper choice of multilayer parameters allows mitigation of the negative impact of refraction and allows achievement of high diffraction efficiency even for a highly asymmetrical geometry.

Optimization of the MBG design should be performed in terms of the asymmetry parameter which in turn ought to be defined by the whole spectrograph design. In order to achieve the highest possible efficiency, rigorous efficiency simulations should be performed for each particular case. Nevertheless, a few general recommendations for an optimization process can be given. First, the period of the grating should be smaller than the extinction length of the soft x-ray radiation in the ML coating. Such a design provides high groove transparency and results in efficiency improvement by a factor of 2 or 3 as compared to long-period MBGs. Secondly, a MBG should be optimized for high order operation since this can provide improvement of spectral resolution or reduction of asymmetry and efficiency improvement without resolution losses. Third, multilayer parameters should be optimized in a way which would reduce the impact of the asymmetry on the grating efficiency. Multilayers with short d-spacing and small Γ-ratio are preferable since they result in lower asymmetry and reduce refraction and absorption in MBGs.

This work shows a roadmap for the development and optimization of MBGs which are crucial elements for advanced soft x-ray spectroscopy techniques such as RIXS, where both spectral resolution and diffraction efficiency are critical.

Acknowledgments

The authors are indebted to A. Rathsfeld (WIAS, Germany) for cross-checking the efficiency calculations, and we are very grateful to Yu. V. Shvyd'ko (APS, Argonne National Laboratory) for fruitful discussions. This work was supported by the U. S. Department of Energy under contract number DE-AC02-05CH11231.

Disclaimer

#221162 - $15.00 USD Received 20 Aug 2014; revised 7 Jan 2015; accepted 20 Jan 2015; published 17 Feb 2015